15 Jan 2022

Optical Interferometric Force Sensor based on a Buckled Beam

Yan Tang

Jing Guo

Yizheng Chen

Jie Huang
Missouri University of Science and Technology, jieh@mst.edu

Recommended Citation

Y. Tang et al., "Optical Interferometric Force Sensor based on a Buckled Beam," *IEEE Sensors Journal*, vol. 22, no. 2, pp. 1301 - 1308, Institute of Electrical and Electronics Engineers, Jan 2022.
The definitive version is available at https://doi.org/10.1109/JSEN.2021.3130615

Optical Interferometric Force Sensor Based on a Buckled Beam

Yan Tang, Jing Guo, Yizheng Chen, and Jie Huang, *Senior Member, IEEE*

***Abstract*—This paper reports a novel extrinsic Fabry-Perot interferometer (EFPI)-based fiber optic sensor for force measurement. The prototype force sensor consists of two EFPIs mounted on a stainless steel rectangular frame. The primary sensing element, i.e., the first EFPI, is formed between the endface of a horizontally-placed optical fiber and a stainless steel buckled beam. The second EFPI, fashioned between a longitudinally-placed optical fiber and a silver-coated glass beam, is arranged to demonstrate the amplification mechanism of the buckled beam structure. When the sensor is subjected to a tension force, the pre-buckled beam will deflect backward, resulting in a longitudinal/axial displacement of the pre-buckled beam. The axial displacement is further transferred and amplified to a horizontal/vertical deflection at the middle of the buckled beam, leading to a relatively-significant change in the Fabry-Perot cavity length. A force sensitivity of 796 nm/*N* (change in cavity length/Newton) is achieved with a low-temperature dependence of 0.005 *N*/°C. The stability of the sensor is also investigated with a standard deviation of ± 5 nm, corresponding to a measurement resolution of ±0.0064 N. A simulation is conducted to study the axial displacement and stress distribution of the sensor when it is subjected to a tension load of 250 N. It is demonstrated that the maximum stress of the sensor is tremendously reduced attributed to the buckled design, enabling a long service life cycle of the force sensor. The robust and simple-to-manufacture force sensor has great potential in structural health monitoring, robotics control, and oil/ gas refining systems.**

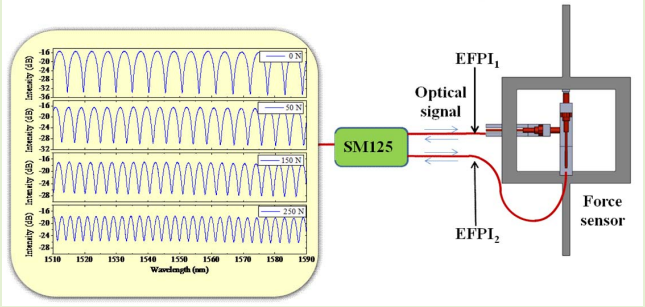

***Index Terms*— Buckled beam, cavity length change, EFPI, optical fiber force sensor.**

I. Introduction

FORCE measurement plays a crucial role in many applications, including civil engineering structures [1], [2], robotics control [3], [4], biomedical and medical surgery [5], [6], and wheel loads of highway vehicles [7]. Various force measurement principles such as piezo-resistive, capacitive, piezoelectric, magnetic, and inductive have been widely studied and adopted with their unique advantages. However, the utilization of these electrical sensors is mainly restricted due to the influence of electromagnetic interference (EMI) and the reduction of signal-to-noise ratio (SNR) with long-distance signal transmission [8]. In the past two decades, the exploitation of fiber-optic sensors provides solutions for overcoming the drawbacks encountered by conventional measurement methods. Further, attributes such as high resolution, high sensitivity, immunity to EMI, light weight, compact size, remote sensing, and multiplexing capabilities enhance the merits of fiber-optic sensors [9]–[11].

In general, most optical fiber based force sensors are based on fiber Bragg gratings (FBGs) because of the ease of wavelength demodulation that is insensitive to the power fluctuation of the light source and the distributed sensing capability [12]. The FBG based force sensors have been finding increasing applications in health monitoring of engineering structures, robotics, and biomedical and medical surgery. An FBG anchor rod force sensor with enhanced sensitivity was presented to realize more accurate and stable measurements in health monitoring of slope anchorage engineering [12]. Another FBG based tension sensor for anchor rope was applied to measure the dynamic forces on anchor ropes for impact test of rockfall protection barriers with the benefits of improved sensitivity and temperature compensation [13]. The FBG sensors take a large proportion in force measurement of cable forces for the prestressing tendons in prestressed concrete structures [1], [14], [15] and bridge cable of suspension bridges or cable-stayed bridges [16]–[18]. Hu *et al.* [19] designed an FBG force sensor with enhanced sensitivity by

Manuscript received September 28, 2021; revised November 4, 2021; accepted November 4, 2021. Date of publication November 25, 2021; date of current version January 12, 2022. The work of Jie Huang was supported by the Roy A Wilkens Professorship Endowment. The associate editor coordinating the review of this article and approving it for publication was Prof. Santosh Kumar. *(Yan Tang and Jing Guo contributed equally to this work.) (Corresponding author: Jie Huang.)*

Yan Tang, Jing Guo, and Jie Huang are with the Department of Electrical and Computer Engineering, Missouri University of Science and Technology, Rolla, MO 65409 USA (e-mail: jieh@mst.edu).

Yizheng Chen is with the Department of Electrical and Computer Engineering, Clemson University, Clemson, SC 29634 USA.

Digital Object Identifier 10.1109/JSEN.2021.3130615

a strain-reinforcing mechanism. A three-dimensional force sensor based on FBG for robot plantar force measuring was presented to address the concerns encountered with electrical force sensors in robotic devices [20]. A tension sensor, taking advantage of the small size FBG, was innovated to measure the grasping force through stain measurement in a laparoscopic surgical robot [21]. In order to accommodate small confined spaces at the tip of a flexible ureteroscope, a compact triaxial force sensor was devised with four FBGs to measure the contact force during ureteroscopy [22]. However, all these FBG force sensors involve package issues due to the fundamental weakness of glass fibers, resulting in high cost and complex fabrication. A glass-to-metal bond is highly essential for obtaining constant strain transfer for reliable measurement results. The most common method of bonding is epoxy adhesive, which involves issues like zero drift, local sliding, strength reducing, non-uniform distribution of stiffness resulting from aging degradation, or uneven application of epoxy adhesive. In addition, the axial pre-tensioning of the FBG sensor during fabrication or installation is difficult to control for safe operation without damaging the FBG. An extra sensor arrangement as a temperature reference is required because of the high sensitivity to temperature variations. Therefore, the fabrication of FBG based force sensors faces the challenge of serving as a long-term monitoring sensor in real-world applications. Fully distributed fiber optic sensors based on light scatterings, primarily implemented in large-scale objects such as bridge cables as summarized in [23], can continuously measure the force through strain sensing along the object to be measured. However, the aforementioned strain-transfer issue remains, and the cost of associated interrogation equipment for distributed fiber optic sensing is much higher than the interrogators desired for point-sensors.

Benefiting from advantages such as small temperature cross-sensitivity and high resolution and sensitivity, force sensors based on Fabry-Perot Interferometer (FPI) have been studied in recent years. Zhao *et al.* [24] proposed an axial contact force measurement sensor based on intrinsic optical fiber bubble-expanded FPI with a high sensitivity of −750.17 pm/N. Liu *et al.* [25] presented an inline FP micro-cavity plugged by a cantilever taper for strain force measurement with a high force sensitivity of 841.59 nm/N. Force sensors based on optical microfiber asymmetrical FPI were fabricated by combing low reflectivity fiber Bragg grating (LR-FBG) to achieve high sensitivity of 0.221 pm/μN [26], [27]. These intrinsic FPI sensors (i.e., optical fiber inline FPIs) required fusion splicing, taping, or complicated pretreatments during the fabrication process, which may affect the mechanical strength and stability of the sensor. In comparison with the intrinsic FPI sensors, sensors based on extrinsic Fabry-Perot interferometer (EFPI) that do not weaken the properties of optic fiber, could be considered as a good candidate for measuring different physical parameters. It has been successfully investigated to measure the strain [28]–[30], pressure [31]–[33], displacement [34], [35], and inclination [36], [37] with different novel mechanical designs. The EFPI force sensors have also been studied to be implemented in various applications. For instance, a multidimensional miniature EFPI force sensor was designed, calibrated, and experimentally applied to probe the forces during vitreoretinal surgery. The small displacements induced by a small force can lead to a change in the lengths of the Fabry-Perot cavities [38]. Su *et al.* presented a magnetic resonance imaging (MRI) guided robot with an integrated FPI strain sensor to provide high-resolution axial needle insertion force measurement [39]. An EFPI principle guided fiber loop ringdown (FLRD) strain sensor was proposed for sensing tension stress on a post-tensioned rod or the concrete [40]. Therefore, a force sensor based on EFPI displacement measurement will exploit its merit to serve as a force measurement with amiable structure design and packaging.

In this paper, a novel buckled beam-based extrinsic Fabry-Perot interferometer (EFPI) force sensor is reported. The force sensor consists of two EFPI sensors mounted on a stainless steel frame. The horizontal arranged $EFPI_1$ sensor takes advantage of a novel mechanical design to realize the amplification of the axial displacement simultaneously measured by the vertically placed $EFPI_2$ sensor. A main Fabry-Perot cavity is formed by the stainless buckled beam and the end face of a single-mode fiber (SMF). Another Fabry-Perot cavity between the end face of the vertically placed fiber and the glass beam is produced to demonstrate the amplification mechanism. The sensor design and the measurement principle are discussed in Section II. Section III presents the specific calibration experiment through applying incremental loads to establish the relationship between the applied load and the change of the cavity length. A simulation using software Abaqus is performed to quantify the axial displacement and the maximum principal stress of the sensor subjected to a tensile load of 250 N. The designed sensor was also applied to measure the weight of the mass blocks to demonstrate its practical applications.

II. Sensor Design and Measurement Principle

Fig. 1(a) shows a photograph of the novel prototype sensor. The sensor consists of a 304 stainless steel frame with a loading bar at the center of the top and bottom sides, a horizontally placed single-mode optical fiber #1 component, a buckled beam, a longitudinally-mounted single-mode optical fiber #2 component, and a glass beam. Fig. 1(b) shows the schematic illustration of the horizontal buckled beam structure from the top view of the sensor. Fig. 1(c) presents the schematic illustration of the optical fiber #2 component from the left side view of the sensor. The unit of labels shown in Figs. 1(b) and (c) is in millimeter. Fig. 1(d) illustrates a schematic drawing of the buckled beam based EFPI sensor for force sensing.

As illustrated in Fig. 1(b), the primary structure includes the horizontal optical fiber #1, the buckled beam with a rectangular cross-section (length × width × height: 24 mm × 4 mm × 0.2 mm), and the steel frame that is used to fix and package the sensing parts. The optical fiber #1 packaged in a ceramic ferrule is horizontally mounted on an L-shaped steel part screwed on the middle of the left side of the frame. The buckled beam is vertically inserted into the slots of the loading

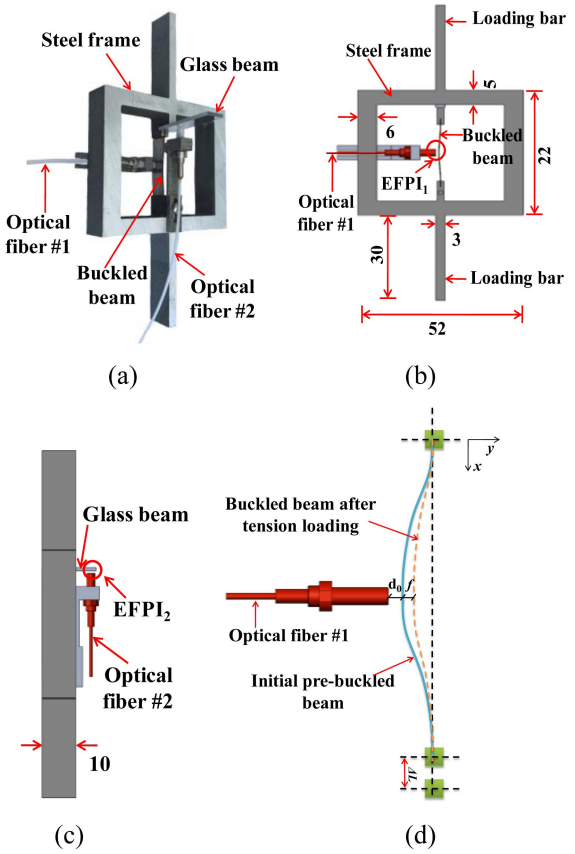

Fig. 1. (a) Photograph of the proposed force sensor. (b) Schematic illustration of the force sensor with optical fiber #1 component and buckled beam (top view)(unit: mm). (c) Schematic illustration of the force sensor with optical fiber #2 component (side)(unit: mm). (d) Schematic illustration of a buckled beam-based EFPI sensor for force sensing. d_0 is the initial distance between optical fiber #1 and the pre-buckled beam, i.e., the initial cavity length setting. f is the backward deflection at the midpoint of the buckled beam after loading.

bars on both sides by 2 mm. Both sides of the buckled beam are laser welded on the loading bars. The stainless beam also serves as a mirror with a reflectivity of 99%. Since the end face of optical fiber #1 is parallel to the center part of the buckled beam, $EFPI_1$ is formed. As shown in Fig. 1(d), the initial distance between fiber #1 and the pre-buckled beam, d_0 is set as the initial cavity length. When the loading bars on both sides are subjected to an axial tension force, the pre-buckled beam will deflect backward and cause an increase denoted as f in the cavity length of the $EFPI_1$.

Based on the Euler buckling theory [41], the deflection shape of the buckled beam can be expressed in the following mathematical model with three assumptions: initially-straight beam, zero eccentricity of applied axial load, and pinned ends.

$$y(x) = -\frac{M_0}{P_{cr}}\cos\left(\sqrt{\frac{P_{cr}}{EI}}x\right) + \frac{M_0}{P_{cr}} \tag{1}$$

where x is the axial displacement of the buckled beam, M_0 is the initial bending moment, E is the modulus of elasticity, and I is the moment of inertia of the beam, $I = bh^3/12$, where b and h are the width and the thickness of the beam, respectively. P_{cr} is the critical buckling load, which is

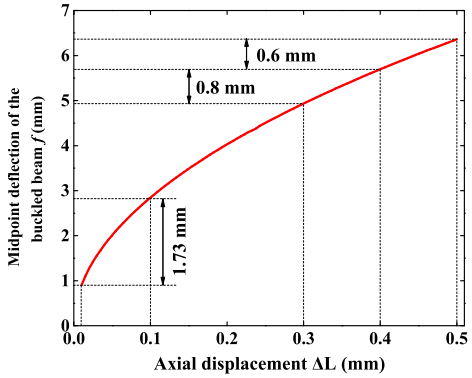

Fig. 2. The relationship between the midpoint deflection of the buckled beam f and the axial displacement along the beam ΔL. The beam is pre-buckled at the initial setting.

expressed as $4\pi^2 EI/(L\text{-}\Delta L)^2$; ΔL is the axial displacement along the buckled beam and L represents the length of the beam. Then, substituting P_{cr} into (1), the relationship between the deflection at the midpoint of the buckled beam f (i.e., $x = L/2$) and the axial displacement of the beam ΔL can be obtained, which is given by

$$f = \frac{M_0 (L - \Delta L)^2}{2\pi^2 EI} \tag{2}$$

A complete analytical solution to equation 1 is provided in [42] by elliptic integral. The deflection at the midpoint of the buckled beam as indicated in equation 2 can be solved by the incomplete elliptic integrals of the second kind [43], which can be given as

$$L = f\int_0^{\pi}\sqrt{1-(k\sin\theta)^2}d\theta \tag{3}$$

where $k^2 = 1\text{-}[(L\text{-}\Delta L)/2f]^2$, d_θ is the infinitesimal width, and θ ranges from 0 to π. It can be noticed that the deflection at the midpoint of the buckled beam f is only associated with the axial displacement of the buckled beam ΔL and the length of the beam L. Fig. 2 plots the deflection at the midpoint of the buckled beam (f) as a function of axial displacement (ΔL). Please note that we assume the length of the beam (L) is 24 mm in the calculation because it is close to the sensor we designed and fabricated. It was found that the center deflection of the beam is much larger than the axial displacement of the beam, revealing that the axial displacement of the beam can be amplified by the buckled structure and transferred to the vertical deflection at the midpoint of the buckled beam. For instance, the midpoint deflection of the buckled beam (i.e., 1.73 mm) is about 17 times greater than the axial displacement (i.e., 0-0.1 mm). The axial displacement from 0.3 to 0.4 mm is amplified by about 8 times. For a typical length of an EFPI cavity, the amplification factor distributes in a range of 6 to 17 regulated by the initial deflection at the center of the buckled beam. The actual use of this nonlinear curve is only a tiny part. According to the typical measurable range of an EFPI cavity length change of hundreds of micrometers, it can be regarded as a linear function.

As presented above, the external force directly leads to the axial displacement and the vertical buckle of the beam.

The deflection at the vertical midpoint of the buckled beam amplifies the axial displacement with a nonlinear increasing curve and can be encoded by the cavity length change of an EFPI sensor. Accordingly, a relationship can be established between the external force and the change of the cavity length through the aforementioned transfer mechanism. The change in cavity length can be obtained by analyzing the interference spectrum. The fast Fourier transform was used to transfer the interference spectrum from the wavelength domain to the frequency domain. Then the absolute cavity length can be correlated to the peak position of the Fourier transform.

As shown in Fig. 1(c), another EFPI based measurement set is secured longitudinally to measure the longitudinal displacement of the sensor directly. An optical fiber #2 packaged in a ceramic ferrule is mounted on one end of an L-shaped part with the other end screwed on the inside of the bottom loading bar of the frame. A rectangular glass beam (length × width × height: 20 mm × 5 mm × 1 mm) is fixed on the inside of the loading bar of the frame. The position of the glass beam is at the top end of the buckled beam. A thin layer of silver (thickness of approximately 80 nm) with a reflectivity of 99% is coated on the bottom surface of the glass beam facing the end face of optical fiber #2. The silver-coated glass beam is used as a mirror. Thus, an $EFPI_2$ is formed between the end face of the fiber and the glass mirror. When the loading bars are subjected to an axial tension force, the relative axial displacement of the sensor will occur between two loading bars, leading to a change in both EFPI cavity lengths. As such, the amplification factor can be calculated by comparing cavity length changes of $EFPI_1$ (i.e., deflection of the buckled beam) and $EFPI_2$(i.e., axial displacement of the buckled beam).

III. Experimental Results and Discussions

The experimental setup that is used to calibrate the force sensor is illustrated in Fig.3. An integrated optical interrogator from Micron Optics (SM125) was used. An internal optical switch encased in the interrogator enables the switching between four channels. The optical fiber of $EFPI_1$ connected to channel one of the SM125 is designated to record and demodulate the deflection of the buckled beam. Another channel connects the optical fiber of $EFPI_2$ to record and demodulate the optical signal caused by the axial displacement of the beam. In order to record and process the interference spectra, a computer connected to the SM125 through an RJ-45 Ethernet cable is used. During the calibration test, the force sensor was tested for tensile loads on a 5982 Electromechanical Testing machine (Instron) with a capacity of 100 kN. The grips were used to fix and apply the tensile load to the loading bar of the sensor. The integrated control panel was used to control the test. The applied load range is increased from 0 to 250 N with a step of 25 N. The calibration loading process is repeated three times.

Fig. 4(a) shows the interference spectra of the $EFPI_1$ measurements for four different loads: 0, 50, 150, and 250 N. Inverse Fourier transform was applied to the recorded spectra in order to obtain the cavity length information as described

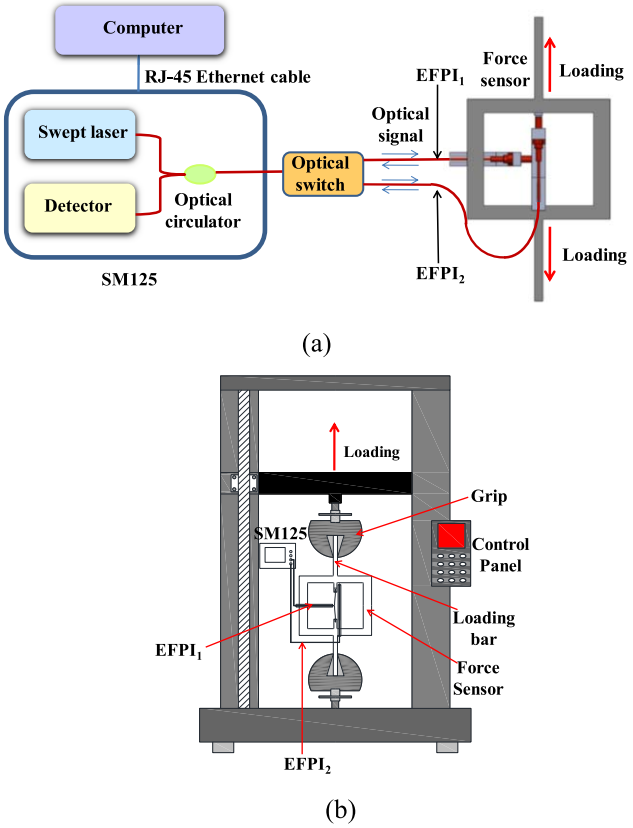

Fig. 3. Schematic diagram of the experimental setup. (a) Two input-output channels are connected to two single-mode optical fibers, forming two EFPIs in the force sensor. (b) The force sensor was tested for tensile loads on a 5982 Electromechanical Testing machine (Instron).

in [35]. The results are shown in Fig. 4(b). We can observe that when the applied load increases, the peak position shifts to the right, revealing that the cavity length enlarges with increasing loading. The magnitude of the peak declines with increasing loading due to the correlation between the magnitude of the peak and the fringe visibility of the interferogram [32], which decreases as the loading increases (i.e., cavity length increases). Fig. 4(c) shows the calibrated relationship between the applied tensile load and the cavity length variation for the buckled beam design of $EFPI_1$ and the longitudinal axial measurement of $EFPI_2$. The average value of the cavity length change is obtained from three separate load tests. It can be found that the change in cavity length of EFPI increases with the applied load for both $EFPI_1$ and $EFPI_2$. The relationship between cavity length variation and the load for $EFPI_1$ and $EFPI_2$ can be simulated and expressed as $y_1 = 0.796\ x$ and $y_2 = 0.0904\ x$ through two linear curve fits, respectively. The R-square of the fittings for the measured data of $EFPI_1$ and $EFPI_2$ are calculated to be 0.9998 and 0.9999, respectively, indicating that good linear relationships are obtained in the two measurements. Consequently, an externally applied load can be determined by the measured cavity length variation of the EFPIs according to the calibrated fitting curve. Fig. 4(d) plots the relationship between the average values of cavity length change of $EFPI_1$ (i.e., the midpoint deflection of the buckled beam, f) and $EFPI_2$ (i.e., axial displacement, ΔL) from three

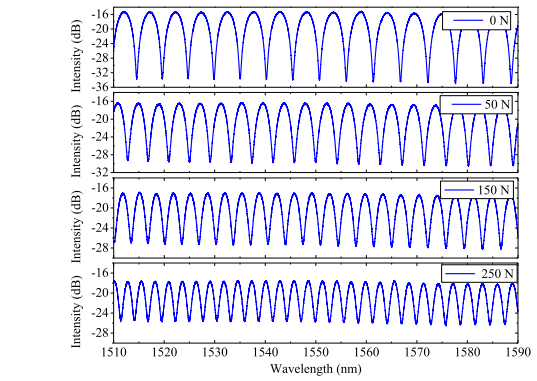

(a)

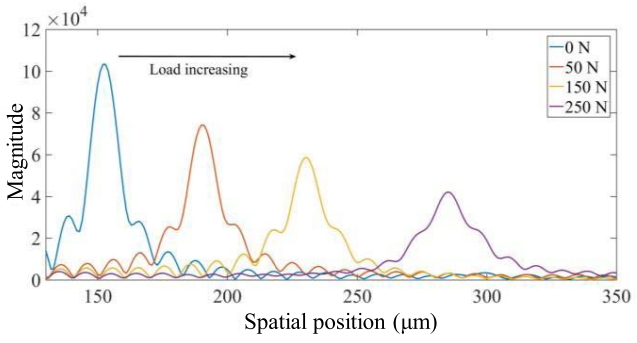

(b)

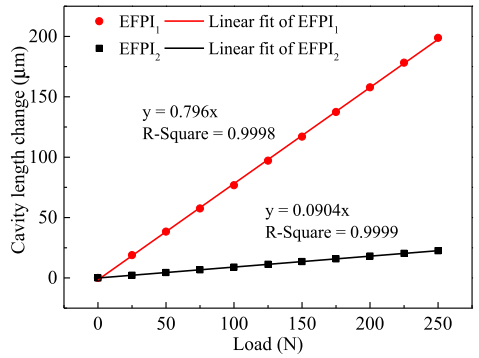

(c)

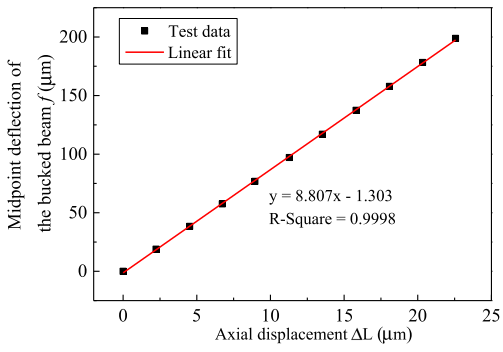

(d)

Fig. 4. (a) Interference spectra of the $EFPI_1$ for four loadings 0, 50, 150, and 250 N. (b) Fourier transform results of the recorded spectra. (c) Measured average cavity length change of $EFPI_1$ and $EFPI_2$ with respect to three repeated loading. (d) The relationship between f (midpoint deflection of the buckled beam) and ΔL (axial displacement) from three repeated loading.

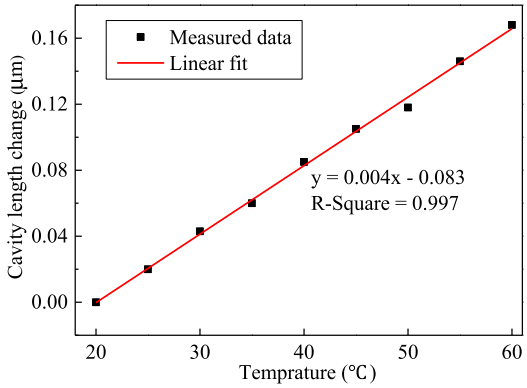

Fig. 5. Measured cavity length change of $EFPI_1$ with respect to temperature.

repeated load tests. A curve fit is applied to the measured data, and the relationship between the cavity length changes resulted from the buckled beam, f, and the axial displacement, ΔL, can be expressed as $y = 8.807\ x - 1.303$. The R-square of the fitting is up to 0.9998. It can be found that amplification of 8.807 is achieved by the buckled beam structure. It also demonstrates experimentally that a tiny section of a nonlinear curve such as the curve in Fig. 2 can be considered as a linear function.

The force sensor was also placed in a temperature-controlled container to investigate the effect of temperature. The container has a measurement accuracy of ±0.5 °C over a range of 65 °C. Fig. 5 shows the measured temperature response from $EFPI_1$. The temperature was raised from 20 °C to 60 °C with a step of 5 °C. A linear relationship between temperature and cavity length change is established, and a temperature sensitivity of 4 nm/°C (change in cavity length/Celsius) is obtained. Taking the load sensitivity of 796 nm/N (change in cavity length/Newton) into consideration, the temperature-force cross-sensitivity of the sensor is 0.005 N/°C. The effect from temperature is small because the cavity length change of the sensor is in the magnitude of tens of micrometers, while the change in cavity length caused by thermal expansion is only in tens or hundreds of nanometers.

The stability of the proposed force sensor with buckled beam $EFPI_1$ was also investigated by placing the sensor in a temperature-controlled container (Beijing Kewei Yongxing Instruments Co. Ltd., DH-360) to maintain the temperature at 20 °C and eliminate environmental interferences. The change of cavity length of $EFPI_1$ was recorded every second for 500 seconds without external loading. Fig. 6 shows the recorded cavity length change and its corresponding equivalent force change. The standard deviation of the cavity length change of $EFPI_1$ within this period was calculated to be ±5 nm, corresponding to an equivalent force change of ±0.0064 N, which is 0.00256% of the full scale of 250 N.

A finite-element analysis using Abaqus was performed to quantify the axial displacement and the Maximum Principal Stress of the proposed force sensor. Fig. 7(a) shows the distribution of the axial displacement when the sensor is subjected to a tensile load of 250 N. The bottom loading

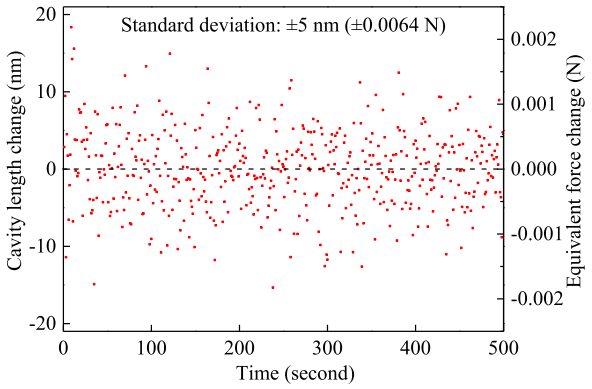

Fig. 6. Measured cavity length change of $EFPI_1$ during a 500 second period.

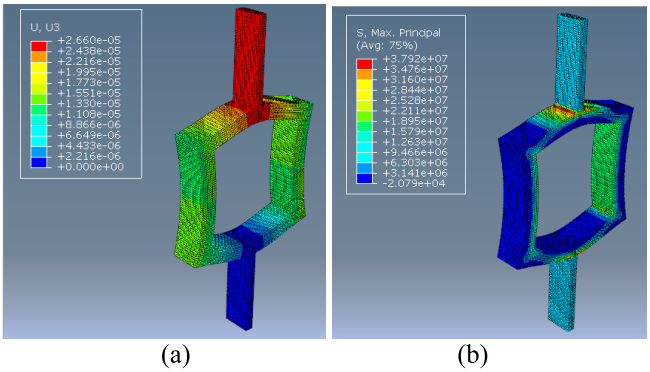

Fig. 7. Simulation results. (a) Axial displacement distribution (unit: m) and (b) Maximum Principal Stress distribution of the frame when the sensor is subjected to a tensile load of 250 N (unit: Pa).

bar colored in blue indicates zero value because of rigid constraint. In contrast, the region around the top-loading bar shows noticeable displacement because of the applied tensile load. As can be observed in the difference between the top and bottom loading bars connected to the rectangle frame, the axial displacement of the force sensor reaches 24.32 μm, which is a 7% difference from 22.54 μm, the measured axial displacement from $EFPI_2$ during the calibration test. The error is mainly due to the differences in metal materials, size deviation, and scratches on the metal of the test.

Fig. 7(b) presents the maximum stress distribution corresponding to the axial displacement plotted in Fig. 7(a). The beam deflection is 194.56 μm which is obtained by multiplying 8.807 times of the axial displacement of 24.32 μm. The corresponding Maximum Principal Stress is simulated as 37.92 MPa shown in red and happens at two connection corners of the loading bar and rectangle frame. If the axial displacement (or cavity length change) is expected to reach 194.56 μm without amplifying in the buckling structure, the maximum stress of the sensor will increase to 334 MPa, which is approaching the tensile strength of 304 steel, 515 MPa. According to the stress life (S-N) curve of a typical 304 stainless steel [44], the life span of the sensor will be tremendously reduced if the maximum stress of the sensor is 334 MPa. Therefore, the enormously decreased maximum stress of 37.92 Mpa achieved by the buckled beam structure

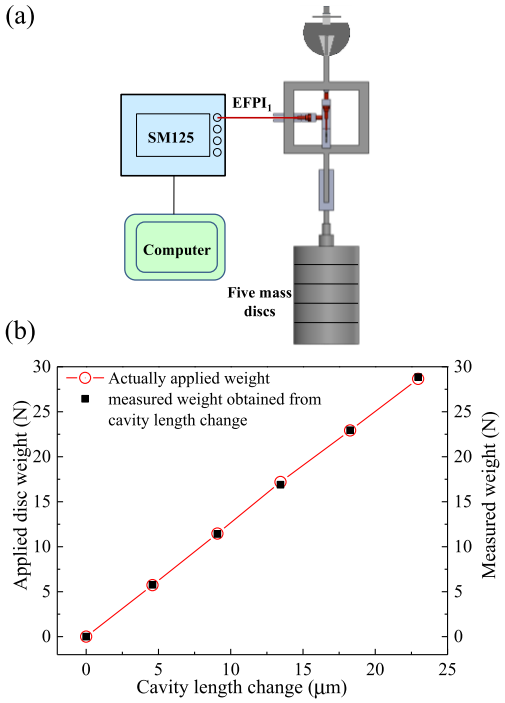

Fig. 8. (a) Schematic diagram of the experimental setup with $EFPI_1$ only. (b) The change in cavity length of $EFPI_1$ with respect to applied disc weight and measured weight, respectively.

releases the fatigue wear of the entire frame and significantly prolongs the service life of the EFPI force sensor.

An experiment for measuring the weight of the mass discs was also conducted to verify the practicability of the proposed EFPI force sensor based on buckled beam. Fig. 8(a) illustrates the schematic diagram of the experimental setup with $EFPI_1$ connected to an interrogator SM125. Five identical stainless steel discs were employed as loading masses, with each in diameter of 40 mm and height of 60 mm. The weight applied to the bottom loading bar was increased from 0 to 28.65 N with a step of 5.73 N (i.e., 585 g). The top-loading bar was fixed during the experiment. The measured cavity length change (bottom scale) from $EFPI_1$ with respect to the applied disc weight (left side scale) is plotted in Fig. 8b. The measured weight (right side scale in Fig. 8b) can be obtained by substituting the measured cavity length change into the calibrated curve $y = 0.796x$ (where y is the measured cavity length change, x is the measured weight). It can be observed that the measured weight matches very well with the applied disc weight, indicating a successful test of the reported EFPI force sensor.

IV. Conclusion

In conclusion, a novel EFPI-based fiber-optic sensor for force measurement using a buckled beam was presented. Attributed to the buckled beam's amplification mechanism, the sensor's force sensitivity was improved by transferring the axial displacement to the center deflection of the beam. We obtained a force sensitivity of 796 nm/N (change in cavity length/Newton) and an amplification factor of 8.807. Moreover, the force sensitivity of the sensor is reconfigurable by changing the initial mid-point deflection of the beam.

The temperature-force cross-sensitivity of the sensor was demonstrated to be 0.005 N/°C. The stability of the sensor was also demonstrated to be ±5 nm, corresponding to a measurement resolution of ±0.0064 N. In addition, the maximum principal stress of the frame was drastically reduced by the buckled beam design so that the service life of the proposed force sensor could be significantly prolonged. The experimental test demonstrated that the measured weight of the discs matched well with the weight of the actual disc, indicating that the reported sensor is able to measure the force with high accuracy in practical applications. The force measurement range and the size of the sensor can be easily reconfigured by adjusting the size of the beam, enabling force measurement for different scenarios.

REFERENCES

[1] M. Perry, Z. Yan, Z. Sun, L. Zhang, P. Niewczas, and M. Johnston, "High stress monitoring of prestressing tendons in nuclear concrete vessels using fibre-optic sensors," *Nucl. Eng. Des.*, vol. 268, pp. 35–40, Mar. 2014.

[2] K. M. Platzer, C. Wendeler, R. Brändle, and M. Stolz, "Experimental investigation of forces along anchors subjected to dynamic loading under tension and compression in field tests," *Can. Geotech. J.*, vol. 57, no. 5, pp. 770–782, May 2020.

[3] A. Bajo and N. Simaan, "Hybrid motion/force control of multi-backbone continuum robots," *Int. J. Robot. Res.*, vol. 35, no. 4, pp. 422–434, Apr. 2016.

[4] G. Palli, L. Moriello, U. Scarcia, and C. Melchiorri, "Development of an optoelectronic 6-axis force/torque sensor for robotic applications," *Sens. Actuators A, Phys.*, vol. 220, pp. 333–346, Dec. 2014.

[5] P. Saccomandi, E. Schena, C. Oddo, L. Zollo, S. Silvestri, and E. Guglielmelli, "Microfabricated tactile sensors for biomedical applications: A review," *Biosensors*, vol. 4, no. 4, pp. 422–448, Nov. 2014.

[6] A. Trejos, R. Patel, and M. Naish, "Force sensing and its application in minimally invasive surgery and therapy: A survey," *Proc. Inst. Mech. Eng. C, J. Mech. Eng. Sci.*, vol. 224, no. 7, pp. 1435–1454, Jul. 2010.

[7] R. B. Malla, A. Sen, and N. W. Garrick, "A special fiber optic sensor for measuring wheel loads of vehicles on highways," *Sensors*, vol. 8, no. 4, pp. 2551–2568, Apr. 2008.

[8] Q. Liang *et al.*, "Multi-component FBG-based force sensing systems by comparison with other sensing technologies: A review," *IEEE Sensors J.*, vol. 18, no. 18, pp. 7345–7357, Sep. 2018.

[9] Z. Chen, G. Hefferman, and T. Wei, "Terahertz-range weak reflection fiber optic structures for sensing applications," *IEEE J. Sel. Topics Quantum Electron.*, vol. 23, no. 2, pp. 246–251, Mar. 2017.

[10] D. Jia, Y. Zhang, Z. Chen, H. Zhang, T. Liu, and Y. Zhang, "A self-healing passive fiber Bragg grating sensor network," *J. Lightw. Technol.*, vol. 33, no. 10, pp. 2062–2067, May 15, 2015.

[11] Y. Guo, L. Xiong, and H. Liu, "Research on the durability of metal-packaged fiber Bragg grating sensors," *IEEE Photon. Technol. Lett.*, vol. 31, no. 7, pp. 525–528, Apr. 1, 2019.

[12] J. Fu, Y. Guo, and P. Li, "A fiber Bragg grating anchor rod force sensor for accurate anchoring force measuring," *IEEE Access*, vol. 8, pp. 12796–12801, 2020.

[13] J. Huang, Z. Zhou, D. Zhang, J. Chen, L. Li, and X. Deng, "Design and application of a fiber Bragg grating tension sensor for anchor rope," *Adv. Mech. Eng.*, vol. 5, Jan. 2013, Art. no. 125404.

[14] S. Kim, Y. Park, S. Park, K. Cho, and J.-R. Cho, "A sensor-type PC strand with an embedded FBG sensor for monitoring prestress forces," *Sensors*, vol. 15, no. 1, pp. 1060–1070, Jan. 2015.

[15] J.-M. Kim, H.-W. Kim, S.-Y. Choi, and S.-Y. Park, "Measurement of prestressing force in pretensioned UHPC deck using a fiber optic FBG sensor embedded in a 7-wire strand," *J. Sensors*, vol. 2016, pp. 1–9, Dec. 2016.

[16] D. Li, Z. Zhou, and J. Ou, "Dynamic behavior monitoring and damage evaluation for arch bridge suspender using GFRP optical fiber Bragg grating sensors," *Opt. Laser Technol.*, vol. 44, no. 4, pp. 1031–1038, Jun. 2012.

[17] R. Zheng, L. Liu, X. Zhao, Z. Chen, C. Zhang, and X. Hua, "Investigation of measurability and reliability of adhesive-bonded built-in fiber Bragg grating sensors on steel wire for bridge cable force monitoring," *Measurement*, vol. 129, pp. 349–357, Dec. 2018.

[18] F. Li, Y. Du, X. Sun, and W. Zhao, "Sensing performance assessment of twisted CFRP with embedded fiber Bragg grating sensors subjected to monotonic and fatigue loading," *Sens. Actuators A, Phys.*, vol. 271, pp. 153–161, Mar. 2018.

[19] D. T. Hu, S. K. Lv, Y. X. Guo, H. G. He, and J. Y. Liu, "A fiber Bragg grating force sensor with sensitization structure," *IEEE Sensors J.*, vol. 21, no. 3, pp. 3042–3048, Feb. 2021.

[20] L. Xiong, G. Jiang, Y. Guo, and H. Liu, "A three-dimensional fiber Bragg grating force sensor for robot," *IEEE Sensors J.*, vol. 18, no. 9, pp. 3632–3639, May 2018.

[21] R. Xue, B. Ren, J. Huang, Z. Yan, and Z. Du, "Design and evaluation of FBG-based tension sensor in laparoscope surgical robots," *Sensors*, vol. 18, no. 7, p. 2067, Jun. 2018.

[22] Y. Deng, T. Yang, S. Dai, and G. Song, "A miniature triaxial fiber optic force sensor for flexible ureteroscopy," *IEEE Trans. Biomed. Eng.*, vol. 68, no. 8, pp. 2339–2347, Aug. 2021.

[23] G. Uva, F. Porco, A. Fiore, and G. Porco, "Structural monitoring using fiber optic sensors of a pre-stressed concrete viaduct during construction phases," *Case Stud. Nondestruct. Test. Eval.*, vol. 2, pp. 27–37, Oct. 2014.

[24] Y. Zhao, F. Xia, M.-Q. Chen, R.-J. Tong, and Y. Peng, "Optical fiber axial contact force sensor based on bubble-expanded Fabry–Pérot interferometer," *Sens. Actuators A, Phys.*, vol. 272, pp. 318–324, Apr. 2018.

[25] Y. Liu, C. Lang, X. Wei, and S. Qu, "Strain force sensor with ultra-high sensitivity based on fiber inline Fabry–Pérot micro-cavity plugged by cantilever taper," *Opt. Exp.*, vol. 25, no. 7, pp. 7797–7806, Apr. 2017.

[26] Y. Gong *et al.*, "Highly sensitive force sensor based on optical microfiber asymmetrical Fabry–Pérot interferometer," *Opt. Exp.*, vol. 22, no. 3, pp. 3578–3584, Feb. 10, 2014.

[27] C. Yu, X. Chen, Y. Gong, Y. Wu, Y. Rao, and G. Peng, "Simultaneous force and temperature measurement using optical microfiber asymmetrical interferometer," *Photonic Sensors*, vol. 4, no. 3, pp. 242–247, Sep. 2014.

[28] Y. Du, Y. Chen, C. Zhu, Y. Zhuang, and J. Huang, "An embeddable optical strain gauge based on a buckled beam," *Rev. Sci. Instrum.*, vol. 88, no. 11, Nov. 2017, Art. no. 115002.

[29] C. Zhu, Y. Chen, Y. Zhuang, F. Tang, and J. Huang, "An embeddable strain sensor with 30 nano-strain resolution based on optical interferometry," *Inventions*, vol. 3, no. 2, p. 20, Apr. 2018.

[30] Y. Du, Y. Chen, Y. Zhuang, C. Zhu, F. Tang, and J. Huang, "Probing nanostrain via a mechanically designed optical fiber interferometer," *IEEE Photon. Technol. Lett.*, vol. 29, no. 16, pp. 1348–1351, Aug. 15, 2017.

[31] C. Zhu, Y. Chen, Y. Zhuang, G. Fang, X. Liu, and J. Huang, "Optical interferometric pressure sensor based on a buckled beam with low-temperature cross-sensitivity," *IEEE Trans. Instrum. Meas.*, vol. 67, no. 4, pp. 950–955, Apr. 2018.

[32] Q. Zhang, J. Lei, Y. Chen, Y. Wu, C. Chen, and H. Xiao, "3D printing of all-glass fiber-optic pressure sensor for high temperature applications," *IEEE Sensors J.*, vol. 19, no. 23, pp. 11242–11246, Dec. 2019.

[33] C. Zhu, Y. Chen, R. E. Gerald, and J. Huang, "Probing changes in pressure with subpascal resolution using an optical fiber Fabry–Pérot interferometer," *IEEE Trans. Instrum. Meas.*, vol. 69, no. 9, pp. 6556–6563, Sep. 2020.

[34] C. Zhu and J. Huang, "An optical fiber extrinsic Fabry–Pérot interferometer based displacement sensor with centimeter measurement range," *Sensors Smart Struct. Technol. Civil, Mech., Aerosp. Syst.*, vol. 10598, p. 105983J, Mar. 30, 2018.

[35] C. Zhu *et al.*, "A displacement sensor with centimeter dynamic range and submicrometer resolution based on an optical interferometer," *IEEE Sensors J.*, vol. 17, no. 17, pp. 5523–5528, Sep. 2017.

[36] Y. Zhuang, Y. Chen, C. Zhu, R. E. Gerald, and J. Huang, "Probing changes in tilt angle with 20 nanoradian resolution using an extrinsic Fabry–Pérot interferometer-based optical fiber inclinometer," *Opt. Exp.*, vol. 26, no. 3, pp. 2546–2556, Feb. 5, 2018.

[37] Y. Zhuang, Y. Chen, C. Zhu, R. E. Gerald, Y. Tang, and J. Huang, "A high-resolution 2-D fiber optic inclinometer for structural health monitoring applications," *IEEE Trans. Instrum. Meas.*, vol. 69, no. 9, pp. 6544–6555, Sep. 2020.

[38] X. Liu, I. I. Iordachita, X. He, R. H. Taylor, and J. U. Kang, "Miniature fiber-optic force sensor based on low-coherence Fabry–Pérot interferometry for vitreoretinal microsurgery," *Biomed. Opt. Exp.*, vol. 3, no. 5, pp. 1062–1076, May 2012.

[39] H. Su, M. Zervas, G. A. Cole, C. Furlong, and G. S. Fischer, "Real-time MRI-guided needle placement robot with integrated fiber optic force sensing," in *Proc. IEEE Int. Conf. Robot. Automat.*, May 2011, pp. 1583–1588.

[40] M. Ghimire, C. Wang, K. Dixon, and M. Serrato, "*In situ* monitoring of prestressed concrete using embedded fiber loop ringdown strain sensor," *Measurement*, vol. 124, pp. 224–232, Aug. 2018.
[41] H. E. Lindberg and A. L. Florence, *Dynamic Pulse Buckling: Theory and Experiment*, vol. 12. Dordrecht, The Netherlands: Springer, 1987.
[42] A. Midha, S. G. Bapat, A. Mavanthoor, and V. Chinta, "Analysis of a fixed-guided compliant beam with an inflection point using the pseudo-rigid-body model concept," *J. Mech. Robot.*, vol. 7, no. 3, Aug. 2015, Art. no. 031007.
[43] P. F. Byrd and M. D. Friedman, *Handbook of Elliptic Integrals for Engineers and Physicists*. Berlin, Germany: Springer, 2013.
[44] *North American Stainless*. Accessed: Aug. 24, 2021. [Online]. Available: https://www.integritystainless.com/wp-content/uploads/2016/07/NAS-HR-Grade-304-304L-304H.pdf

Yan Tang received the B.S. and master's degrees in hydraulic and hydropower engineering from Lanzhou Jiaotong University, Lanzhou, China, in 2008 and 2011, respectively, and the Ph.D. degree in civil engineering from the Missouri University of Science and Technology, Rolla, MO, USA, in 2017.

She is currently a Postdoctoral Fellow of Electrical and Computer Engineering at the Missouri University of Science and Technology. Her research interest is focused on the innovation and application of smart rock technology for bridge scour monitoring.

Jing Guo received the B.S. degree in environmental science from the China University of Petroleum, Beijing, China, in 2008, and the master's degree in geoscience from the University of Texas at Dallas, USA, in 2015. She is currently pursuing the Ph.D. degree in electrical engineering with the Missouri University of Science and Technology, Rolla, MO, USA.

Her research interest is focus on microwave coaxial cable sensor application in geotechnical aspects.

Yizheng Chen received the B.S. and master's degrees in civil engineering from Tongji University, Shanghai, China, in 2009 and 2011, respectively, and the Ph.D. degree in civil engineering from the Missouri University of Science and Technology, Rolla, MO, USA, in 2017.

He is currently a Research Assistant Professor of Electrical and Computer Engineering at Clemson University, Clemson, SC, USA. His research interest is focused on optical fiber corrosion sensors.

Jie Huang (Senior Member, IEEE) received the Ph.D. degree in electrical engineering from Clemson University, Clemson, SC, USA, in 2015. Dr. Huang is the Roy A. Wilkens Endowed Associate Professor of Electrical and Computer Engineering at the Missouri University of Science and Technology, Rolla, MO, USA. He established the Lightwave Technology Laboratory (LTL) with a strong track record of sustained research funding, high-quality journal publications, and state-of-the-art research infrastructure with cutting-edge capabilities. He authored or coauthored over 100 refereed articles, 70 conference papers, one book chapter, and ten U.S. patent applications, all in the arena of advanced sensors. His research focuses on the development of optical and microwave sensors and instrumentation for applications in energy, intelligent infrastructures, clean environments, biomedical sensing, and harsh environments.